Effect of Temperature on Freshwater Pay Zone Identification - A Laboratory Study

Mohammed Al-Hamad[1], Mustafa Huwaider[2], Shouxiang Mark Ma[2], and Wael Abdallah[3]

[1]SLB, Schlumberger Dhahran Carbonate Research Centre, 31952 Dhahran, Saudi Arabia.
[2]Saudi Aramco, Reservoir Description & Simulation Department, 31952 Dhahran, Saudi Arabia
[3]SLB, 200 Gillingham Lane, Sugar Land, TX 77478, United States

Abstract. When water is fresh, resistivity contrast between water and hydrocarbon (HC) is low, thus it is difficult to identify HC pay using conventional resistivity-based methods, a typical formation evaluation challenge. The objective of this laboratory study is to evaluate a methodology to enhance the differentiation between oil and fresh water by varying measurement temperatures. When heating a rock/oil/water system, each of the three phases would respond differently to the change in temperature. Ratio of resistivities measured at different temperatures would allow oil to be differentiated from water relatively easily, even when water is fresh. A high-pressure high-temperature resistivity cell was used in this study. Outcrop limestone cores are saturated with water and oil. The resistivity of the cores, at different saturations, were measured at elevated temperatures. The effect of temperature on resistivity changes was found to be function of water saturation. The higher the water saturation, the more reduction in resistivity is noticed. At higher temperature, the resistivity of water and oil found to behave differently. Using the measured data at different temperatures, the resistivity ratio was calculated, by dividing the higher temperature resistivity over the lower temperature one. When plotting the calculated resistivity ratio versus test temperature, similar trend was observed for all the samples, with clear shift, allowing identifying oil from fresh water pay zones. The analysed samples had water saturation ranges from around 10% (close to connate water saturation in a typical dry oil producing interval) to 100% (the water leg). The findings of this study offer a new technique to identify oil bearing zones in freshwater environment, an industrywide challenge. It may also provide insights for geothermal exploration using electromagnetic methods.

1 Introduction

Proper differentiation between water and oil zones is crucial to evaluating oil bearing reservoirs [1]. In high water salinity formations, the task is relatively straight forward and water saturation (S_w) is often quantified by using such as the popular Archie model [2], even across waterflooded intervals where post hydrocarbon (HC) migration water imbibition occurs [3,4]. In low resistivity contrast reservoirs when formation water is fresh, separating water from oil zones becomes difficult, as resistivity is high for both [5-7]. In zones with freshwater, measurements less sensitive to water salinity may be better suited, such as dielectric and NMR logs [8], but the depth of investigation of those are typically shallow [9], thus measurements may not be reservoir representative.

In this study, we present a new technique for pay zone identification and formation evaluation based on resistivity responses among water, oil, and rock minerals when heat is applied [10-13]. Electrical conductivity of both water and oil increase with increase in measurement temperature [14-16]. However, the change in conductivity to crude oil is relatively slow compared to that of water [16]. Hence, when heat is applied to zones saturated with both crude oil and water, each fluid phase will response to the applied heat differently, thus making it easier to be differentiated and evaluated; a solution to address the industrywide challenge of formation evaluation in freshwater environment.

2 Materials and Techniques

2.1 Rock Samples and Fluids

Six carbonate outcrop core samples (five limestones and one dolomite) of 1.5” by 2” were prepared in this study. Porosity (ϕ) was measured with helium based on Boyle’s law and permeability (k) with nitrogen using equipment Coretest AP-608, at a confining stress of 500 psi (Table 1).

Low salinity brine of 10 kppm NaCl and Soltrol 130 refined oil from ChevronPhillips were selected, with density (ρ) measured at 20°C as 1.007 g/cc and 0.749 g/cc,

* Corresponding author: mal-hamad@slb.com

respectively. Brine resistivity (R) was measured as 0.628 ohm.m at 20°C (Table 1).

Table 1. Properties of rock and fluids used in this study.

Sample	ϕ [%]	k [mD] @500 psi	ρ [g/cc] @20oC	R [ohm.m] @20oC
IND115-1-6	16.18	52.03	--	--
IND115-1-7	15.81	45.35	--	--
IND115-2-7	18.12	100.32	--	--
IND115-2-8	18.60	183.21	--	--
IND50-1-3	16.30	46.50	--	--
DSI1-2	10.65	152.54	--	--
Brine 10 kppm	--	--	1.007	0.628
Oil Soltrol130	--	--	0.749	---

2.2 Experimental Procedures

The experimental procedures are listed below,

1. Preparation of core and fluid samples,
2. Measure basic properties of core samples and fluids,
3. Saturate core samples with the prepared brine,
4. Established initial saturations of brine (S_w) and oil (S_o) with a centrifuge,
5. Measure core sample resistivity (R) using a 2-electrode high pressure high temperature (HPHT) cell at 20 KHz with a confining pressure of 1000 psi, at various temperatures; 25°C, 75°C, 100°C, and 135°C.

The above experimental procedures are summarized in Fig. 1,

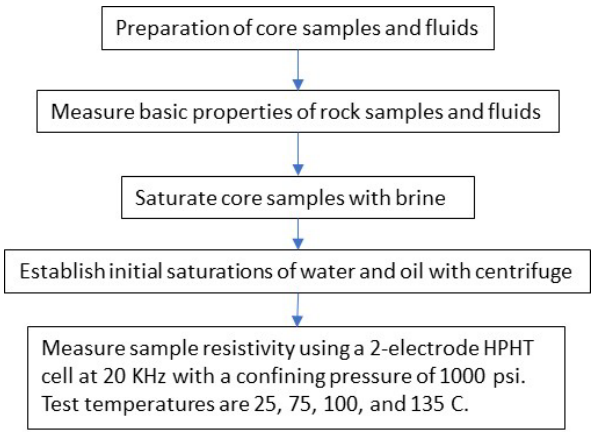

Fig. 1. Experimental procedures.

3 Results and Discussion

3.1 Connate Water Saturation S_w Establishment

To establish core sample partial saturation, fully brine saturated cores were displaced by oil with a centrifuge. The established average water saturations (S_w) at different centrifuge speeds ω are summarized in Table 2. The magnitude of S_w is controlled by the balance between the centrifugal force and capillary force (Eq. 1),

$$f(S_{wc}) \propto \frac{\omega^2 \Delta\rho(r_2{}^2 - r_1{}^2)}{2} = \frac{2\sigma\cos\theta}{r} \quad (1)$$

Where Δρ is the density difference between water and oil, r_2 and r_1 are distances from the center of the centrifuge and the outer and inner faces of the rock sample, ω the speed of the centrifuge, σ water-oil interfacial tension, θ contact angle, and r is the pore size which can be calculated using Eq. 2 [17], if the pore shape is assumed circular [18]

$$r[\mu m] = \sqrt{\frac{8k[\mu m^2]}{\emptyset}} \quad (2)$$

Table 2. Average water saturations for the core samples.

Sample	ϕ	k [10^{-3} μm²]	r [μm]	ω [rpm]	Sw [%]
IND115-1-6	0.1618	52.03	1.5934	1.2k	61.69
IND115-1-7	0.1581	45.35	1.5049	800	82.55
IND115-2-7	0.1812	100.3	2.0907	7k, 8k, 9k	28.77
IND50-1-3	0.1630	183.2	1.5008	5.3k	45.93
DSI1-2	0.1065	46.50	3.3628	9k	12.67

Intuitively, water saturation S_w (z axis of Fig. 2) decreases with increasing centrifuge speed (y axis), and the higher the rock quality or the larger the pore size r (x axis), the lower the S_w (Fig. 2).

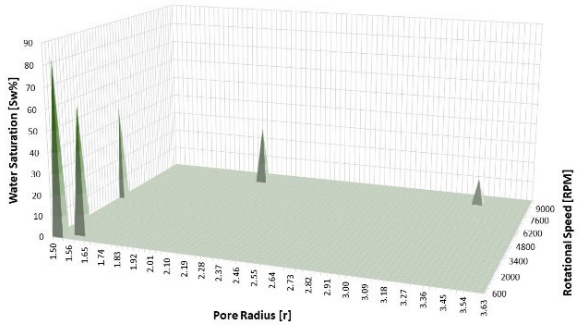

Fig. 2. Changes in water saturation S_w (z axis) with rock quality (pore radius r in x axis) and centrifuge speed (y axis).

3.2 Measurements Results and Analysis

3.2.1 Effect of Temperature on Resistivity at S_w=1

Archie developed an empirical relationship between water saturation S_w and rock resistivities, Eq. 3 [2], which is the foundation of modern petrophysics.

$$S_w^n = \frac{R_0}{R_t} = \frac{R_w}{R_t}\frac{1}{\emptyset^m}, \text{ where } R_0 = \frac{R_w}{\emptyset^m} \quad (3)$$

Where ϕ is the porosity, m the cementation factor (often defaulted to 2.0), n the saturation exponent (another parameter often defaulted to 2.0), R_w, R_0, and R_t are resistivities of water, rock at S_w=1, and rock at S_w<1, respectively.

Effect of temperature on R_w

Effect of temperature on R_w is well documented and have been approximated by using the below Arps Eq. 4 [19],

$$R_{w2} = R_{w1}\frac{T_1[°F]+6.77}{T_2[°F]+6.77} \quad (4)$$

Where T_1 is the lower temperature and T_2 is the higher temperature, for a reservoir or in the lab for a core sample. In this section, we will investigate effect of temperature on rocks fully saturated with brine, i.e, R_0.

Core sample IND115-2-8 is fully saturated with brine, then loaded in a high pressure and high temperature (HPHT) resistivity cell, so that resistivity measurements can be conducted at elevated temperatures; following the below procedures;

1. The sample was first kept in the HPHT cell at a temperature T= 25ºC for 24 hr, after which the resistance was measured for 30 mins, until stable resistivity readings were noticed and recorded with an average value of R_0=19.43 ohm.m.
2. The sample was then heated to T=75ºC and was kept for 24 hrs to ensure stability. The resistivity measurements were then taken for over 30 mins and recorded with an average value of R_0=9.41 ohm.m.
3. The temperature was then increased to T=100ºC for 24 hrs and resistivity was measured with an average value of R_0=6.73 ohm.m.
4. Finally, the sample was heated to the maximum allowable temperature of the instrument at T=135ºC and was allowed to stabilize for 24 hr. The measured resistance data was R_0=5.03 ohm.m.

Experimental data from the above experiments is summarized in Table 3 and plotted in Fig. 3, which shows that the limited four data point follow a logarithmic relationship between R_0 and T, and the trend is same as the Arps model (Eq. 4) using the measured R_w (Table 1), and the commonly used log interpretation chart (Fig. 4).

Table 3. Measured average resistivity at each temperature.

T [ºC]	25	75	100	135
R_0 measured (ohm.m)	19.43	9.41	6.73	5.03

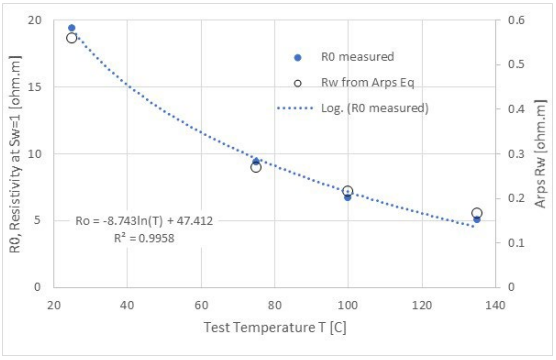

Fig. 3. Resistivity decreases with increasing measurement temperature, fully water saturated sample INC115-2-8.

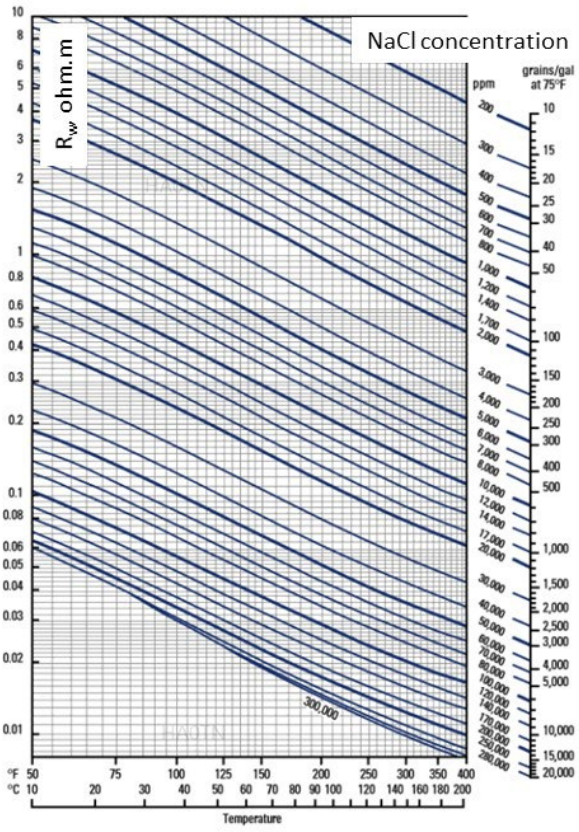

Fig. 4. Effect of temperature and NaCl concertation on water resistivity (Schlumberger log interpretation chartbook [20]).

3.2.2 Effect of Temperature on Resistivity at Sw<1

To study effect of temperature on core resistivity R_t at partial saturation, S_w<1, the samples were loaded in the HPHT resistivity cell, where the resistivity was measured at elevated temperatures, starting from 25ºC to 135ºC. Similar as the R_0 tests at S_w=1, where the cell was kept for 24 hrs at a specific temperature, before measurement was taken over a 30 min time, that the average resistivity value was reported. First, sample IND115-1-7 was loaded, and its resistivity was measured at elevated temperatures. The measured resistivity decreased with higher temperature being applied, and the reported average resistivity values were 44.30, 20.03, 15.83 and 11.72 ohm.m, at 25, 75, 100 and 135ºC, respectively. The results are shown in Figure 5 and summarized in Table 4. Comparing the trend to the

fully brine saturated core (IND115-2-8, Table 3), very similar trend can be noticed, though resistivity is higher due to lower water saturation.

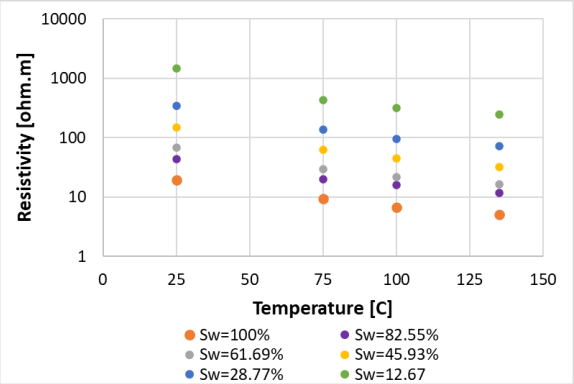

Fig. 5. Resistivity decreases with increasing measurement temperature for samples at S_w=1, as well as S_w<1.

Table 4. Measured average resistivity for the low water saturated samples at each temperature.

Sample	Sw [%]	T [ºC]	Average Resistivity [ohm.m]
IND115-1-7	82.55	25	44.30
		75	20.03
		100	15.83
		135	11.72
IND115-1-6	61.69	25	68.67
		75	29.77
		100	21.77
		135	16.47
IND50-1-3	45.93	25	148.02
		75	62.39
		100	44.34
		135	32.39
IND115-2-7	28.77	25	340.63
		75	137.88
		100	96.49
		135	71.94
DSI1-2	12.67	25	1477.84
		75	432.11
		100	314.25
		135	246.3

3.3 Data Analysis

If the resistivity of the core sample at a lower temperature T1 is R_{T1} and at a higher temperature T2 is R_{T2}. Then, to simplify data analysis, a resistivity factor (RF) can be defined by ratio the two.

$$RF = \frac{R_{T2}}{R_{T1}} \qquad (5)$$

In order to compare resistivity results of the different core samples with different water saturations, the resistivity data was normalized by using Eq. 5, with T_1 is set at 25ºC, and are summarized in Table 5. By plotting the resistivity factors versus water saturations, at each T_2/T_1 ratio, good relations can be observed (Figure 6), which allows prediction of water saturation from RF by using,

$$\mathrm{RF} = \mathrm{a}\, S_w + \mathrm{b} \qquad (6)$$

or

$$S_w = \frac{\mathrm{RF} - \mathrm{b}}{a} \qquad (7)$$

Where a and b are variables with respect to the temperature ratios and their values are shown in Fig 6, for each fitting line. It is worth mentioning that there was a slight deviation noticed at the lowest water saturation, as shown in Fig 6. This could be due to the different composition of this sample, dolomite, and its response to a temperature change might be different from limestone cores. It is, however, not the subject of this paper.

Table 5. Calculated resistivity factor for all the samples with respected to resistivity measured at 25ºC.

Sample	Sw [%]	T [ºC]	Resistivity Factor
IND115-2-8	100	25	1.000
		75	0.484
		100	0.346
		135	0.259
IND115-1-7	82.55	25	1.000
		75	0.452
		100	0.357
		135	0.265
IND115-1-6	61.69	25	1.000
		75	0.434
		100	0.317
		135	0.240
IND50-1-3	45.93	25	1.000
		75	0.421
		100	0.300
		135	0.219
IND115-2-7	28.77	25	1.000
		75	0.405
		100	0.283
		135	0.211
DSI1-2	12.67	25	1.000
		75	0.292
		100	0.213
		135	0.167

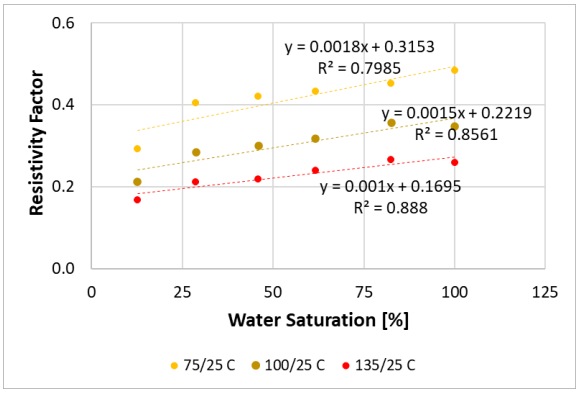

Fig. 6. Resistivity factors versus water saturations for three temperature ratios.

Now taking these variables and plotting them against the temperature rations (Fig.7), the following correlation equations can be obtained (Eq. 8 and Eq. 9)

$$a = -0.0003\,Tr + 0.0028 \quad (8)$$

$$b = -0.0593\,Tr + 0.4805 \quad (9)$$

where Tr is the temperature ratio at which RF is calculated. Now, for each resistivity measurements at two temperatures, Tr is calculated by dividing the higher temperature over the lower temperature, then a and b parameters are calculated using Eqs 8 and 9. After that, using Eq. 7, one can predict the water saturation of the core sample.

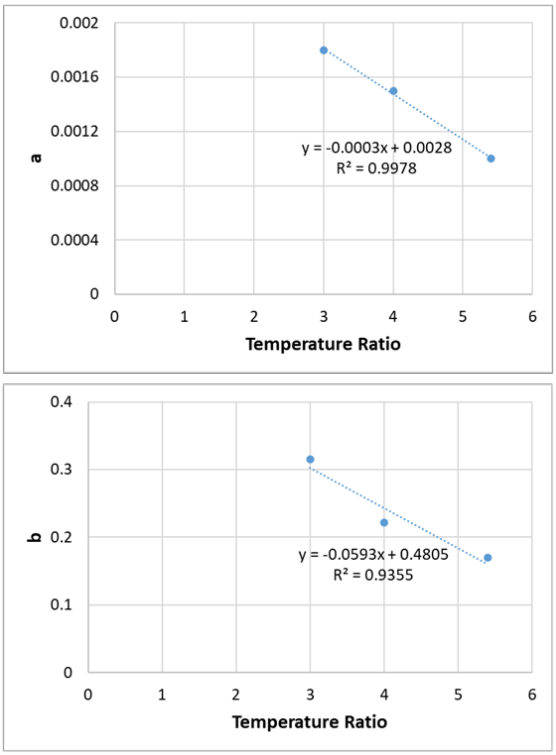

Fig. 7. Slope a and intercept b as function of temperature ratio.

3.3.1 Resistivity Results Validation

To validate the results of the derived correlations, two new tests were prepared and conducted on two new carbonates sample (i.e. IND115-12 and IND115-14). The samples were initially prepared, cleaned and their petrophysical properties were measured, Table 6 summarizes their properties.

Table 6. Petrophysical properties of the validation samples.

Sample	L [cm]	D [cm]	Porosity [%]	Perm [mD]
IND115-12	4.983	3.819	16.26	41.52
IND115-14	4.991	3.814	16.90	56.90

The samples were then fully saturated with 10 kppm NaCl brine, before they were desaturated with Soltrol oil by centrifugation, to water saturations of 26.70% and 47.96% respectively. Then, the samples were loaded separately into the HPHT resistivity cell, and their resistivity were measured at temperatures of 25ºC and 135ºC, and the resistivity factors were then calculated (Table 7).

Table 7. Measured resistivity and calculated resistivity factor for the validation samples.

Sample	Sw [%]	T [ºC]	Resistivity [ohm.m]	Tr	RF
IND115-12	26.7	25	264.91	1	1
		135	50.420	5.4	0.190
IND115-14	47.96	25	166.24	1	1
		135	37.790	5.4	0.220

Now using Tr and RF, Eqs 7, 8, and 9 can be used to calculate water saturation. As can be seen from Table 8 results, very good saturation predictions were obtained, with an average error of around 5%, when compared to the measured water saturation values.

Table 8. Predicted water saturations for the validation samples.

Sample	Temperature Ratio	Resistivity Factor	a	b	PredictedSw [%]
IND115-12	1	1			
	5.4	0.190	0.00118	0.16028	25.18
IND115-14	1	1			
	5.4	0.220	0.00118	0.16028	50.61

3.4 Oil Pay Zone Identification

The results and the developed RF from this study can be used to identify oil pay from water bearing zones. Using Arps equation, Eq. 4, the resistivity of brines at elevated temperatures can be calculated, i.e., previously measured 10 kppm NaCl brine resistivity (0.628 ohm.m at 20ºC) can be converted to resistivity at higher temperatures (75, 100 and 135ºC), as shown in Table 9.

Now, using the brine resistivity results, a formation or core sample true resistivity values can be calculated at elevated temperatures, by rearranging Archie Eq.

$$R_t = \frac{R_w}{S_w^n \, \varphi^m} \quad (10)$$

By assuming a porosity of 20%, and a water saturation of 100%, and a brine resistivity at a temperature, the true resistivity can be calculated (Table 9). Now, RF can be calculated by dividing the true resistivity at higher temperature by that at lower temperature (25°C in this study), and the results are summarized in Table 9.

Table 9. Calculated brine and true resistivities.

T [°C]	Rw [ohm.m]	Rt [ohm.m]	RF
20	0.628	18.158	
25	0.561	16.206	1
75	0.270	7.809	0.482
100	0.215	6.202	0.383
135	0.167	4.815	0.297
200	0.118	3.402	0.210
300	0.081	2.344	0.145
400	0.062	1.788	0.110

When porosity and water saturation change, the true resistivity values will also change, though RF remain the same. Therefore, these RFs can be treated as modelled values. This concept can be then used to identify oil from water bearing zones. As in water bearing zones, or in core samples at S_w=1, similar RFs, at respective temperatures, were observed (comparing results in Table 5 and Table 9). For core samples at S_w<1, clear differences can be noted between the RFs in Table 5 to the modelled RFs in Table 9. By taking the RF difference to the modelled values, one can identify oil from water bearing zone. The higher the difference, the more oil is in the formation/core, and vice versa. Zero difference will indicate that the formation/core is fully saturated with water. For example, taking the difference between the resistivity factor data at 75°C from Table 5 with the modelled data in Table 9, clear trend can be seen with water saturations, as shown in Fig.8. Fig.9 summarizes the proposed workflow for oil pay zone identification.

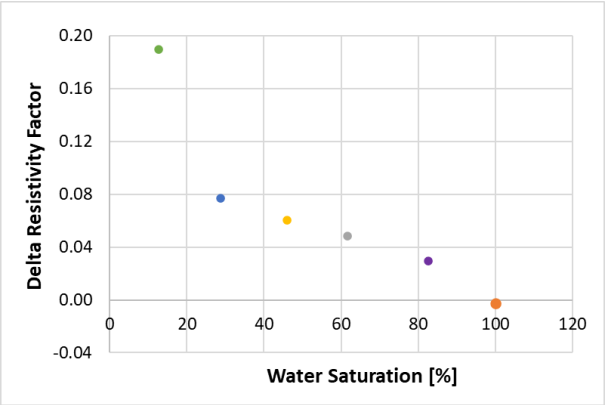

Fig. 8. Resistivity factor difference versus water saturations.

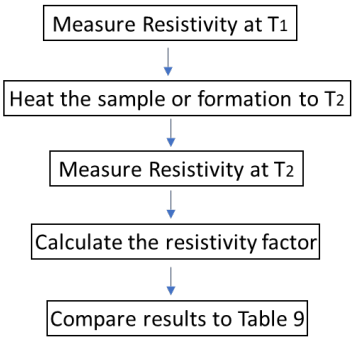

Fig. 9. Workflow for oil pay zone identification.

4 Conclusion

Identification of water and oil-bearing zones in a reservoir is essential for hydrocarbon exploration. In high water salinity formations, it is relatively easy to by using the Archie Eq. When the formation water is fresh, the contrast in resistivity is low. In this case, it is difficult to identify water from oil zones.

In this study, a new method is developed to identify oil and water bearing zones in freshwater/low salinity environments. The method relies on using the resistivity of the formation/core at different temperatures and using a normalized resistivity factor.

Number of carbonates rock samples were investigated, at different water/oil saturations. The method showed its robustness to predict water saturation values in comparison to the true values, which can be used for oil pay zone identifications.

The authors would like to thank Ahmad AlZoukani, Farhan Ali and Vijaya Puvvala for their valuable contributions to this study.

k: permeability
R: resistivity
S: saturation
ϕ: porosity
ρ: density

References

1. Y.K. Saadu, C.N. Nwankwo, Petrophysical evaluation and volumetric estimation within Central swamp depobelt, Niger Delta, using 3-D seismic and well logs, Egyptian Jour. Petrol., **27**(4), 531-539 (2018).
2. G.E. Archie. The electrical resistivity log as an aid in determining some reservoir characteristics. Trans. Of AIME 146 (1): 54-146 (1942).
3. A. Sunbul, S. Ma, A. Hajari, A. Srivastava, R. Ramamoorthy. Quantifying remaining oil by use of slim-hole resistivity measurement in mixed salinity environments –a pilot field test, Paper SPE 97489, Int'l IOR Conference in Asia Pacific, Kuala Lumpur, Malaysia, December (2005).
4. S. Ma, A. Al-Hajari, D. Kersey, J. Funk, L. Bruno. Fit-for-purpose laboratory core analysis program for field reservoir saturation monitoring, Paper SPE 105301, The Middle East Oil, Gas and Geosciences Show, Manama, Bahrain, February (2007)
5. C. B. Ayadiuno, S. Khan, A. A. AlAbbad, F. AlMohsen. Investigating Low Resistivity-Low Contrast Resistivity Pay in a Permo-Carboniferous Reservoir, Central Saudi Arabia. SPE 188887, Abu Dhabi International Petroleum Exhibition & Conference, Abu Dhabi, UAE, November (2017).
6. O. Stanley. Challenges in Identifying and Quantifying Hydrocarbons in Thinly Bedded, Laminated, and Low-Resistivity Pay Zones, Paper OTC 24882, Offshore Technology Conference-Asia, Kuala Lumpur, Malaysia, March (2014).
7. K.K. Kyi, H. Hashim. Fresh Water Conundrum in Oil and Gas Reservoirs of Malaysia, Paper SPE 158003, SPE Asia Pacific Oil and Gas Conference and Exhibition, Perth, Australia, October (2012).
8. A. Al-Harbi, D. Schmitt, S. Ma. Toward quantitative remaining oil saturation: determination challenges & techniques, Paper SPE 147651, SPE Annual Technical Conference and Exhibition, Denver, USA, November (2011).
9. P. Zhang, W. Abdallah, G. Wang, S. Ma. Deep dielectric-based water saturation in fresh water & mixed salinity environments, Paper SPWLA-2021-0033, SPWLA 62nd Annual Symposium, Virtual Event, May (2021).
10. M. Al-Huwaider, S. Ma. Formation evaluation with targeted heating, US Patent 11,578,585, February (2023a).
11. M. Al-Huwaider, S. Ma. Heating and evaluating a formation of the earth while drilling a wellbore, US Patent 11,713,651, August (2023b).
12. M. Al-Hamad, W. Abdallah, S. Ma, M. Al-Huwaider. Processes for determining formation salinity and identifying oil bearing zones in freshwater pay zones, US Patent Application 18/483,112, October (2023a).
13. M. Al-Hamad, W. Abdallah, S. Ma, M. Al-Huwaider, A. AlZoukani. Identification of clays in porous media by integrating electromagnetic measurements and temperature gradient analysis, US Patent Application 18/508,376, November (2023b).
14. K. R. Morash, R. D. Thornton, C. H. Saunders. Measurement of the Resistivity of High-Purity Water at Elevated Temperatures, Ultrapure Water, **11**(9), pp. 18-26, December (1994).
15. T.S. Light, S. Licht, A.C. Bevilacqua, K.R. Morash. The Fundamental Conductivity and Resistivity of Water, Electrochemical and Solid-State Letters, **8**(1), E16 (2005).
16. R. Charin, G. Chaves, K. Kashefi, R., Alves, F. Tavares, M. Nele. Crude Oil Electrical Conductivity Measurements at High Temperatures: Introduction of Apparatus and Methodology, Energy & Fuels, **31** (4), 3669-3674 (2017).
17. S. Ma, M. Jiang, N. Morrow. Correlation of capillary pressure relationships and calculations of permeability, SPE 22685, SPE Annual Technical Conference and Exhibition, Dallas, October (1991).
18. J. Ma, L. Liang, M. Al-Hamad, M. van Steene, S. Ma, W. Abdalla. Aspect ratio dependent pore size distribution from MICP measurement, Paper IPTC-23659, The International Petroleum Technology Conference, Dhahran, Saudi Arabia, February (2024).
19. D. Kennedy. Arps' approximation revisited and revised, Paper SPWLA-5005, SPWLA 61st Annual Logging Symposium, Online, June (2020).
20. Schlumberger, *Schlumberger Log Interpretation Charts*, SMP-7006, Houston, TX (1997).